Energy & Environmental Science

Cobalt Metal Enables Ultrahigh-Efficiency, Long-Life, and Dendrite-Free Aqueous Multivalent Batteries

Journal:	*Energy & Environmental Science*
Manuscript ID	EE-ART-12-2024-006091.R2
Article Type:	Paper
Date Submitted by the Author:	08-Mar-2025
Complete List of Authors:	Chang, Songyang; University of Puerto Rico Rio Piedras Hou, Wentao; University of Puerto Rico Rio Piedras, Department of Chemistry Del Valle-Perez, Angelica; Universidad de Puerto Rico Recinto de Rio Piedras Ullah, Irfan; University of Puerto Rico Rio Piedras, Department of Chemistry Du, Xiaoyu; Universidad de Puerto Rico Recinto de Rio Piedras Cunci, Lisandro; University of Puerto Rico, Department of Chemistry Morell, Gerardo; Universidad de Puerto Rico Recinto de Rio Piedras Wu, Xianyong; University of Puerto Rico Rio Piedras, Department of Chemistry

Aqueous rechargeable metal batteries have gained increasing attention as promising candidates for sustainable energy storage, due to their inherent safety, environmental compatibility, and cost-effectiveness. Currently, various multivalent metals have been explored, ranging from iron, manganese, nickel to indium and antimony. However, cobalt metal chemistry has remained largely underexplored. This work highlights the unique advantages of cobalt metal in aqueous electrolytes, demonstrating its exceptionally high efficiency (~99.9%), long life (5.5 months), and favorable spherical morphology. These features enable cobalt to achieve excellent performance even under harsh conditions, including ultrahigh capacities and low current densities, which far outperform many existing metal electrodes. By investigating cobalt plating chemistry and its compatibility with various cathode materials, this study unlocks cobalt's potential to fabricate high-energy, high-power, and long-life aqueous batteries. This work not only bridges the knowledge gap about cobalt metal but also opens new opportunities for energy storage solutions using environmentally friendly aqueous electrolytes.

Cobalt Metal Enables Ultrahigh-Efficiency, Long-Life, and Dendrite-Free Aqueous Multivalent Batteries

Received 00th January 20xx,
Accepted 00th January 20xx

DOI: 10.1039/x0xx00000x

Songyang Chang,[a] Wentao Hou,[a] Angelica Del Valle-Perez,[a] Irfan Ullah,[a] Xiaoyu Du,[a] Lisandro Cunci,[a] Gerardo Morell,[b] and Xianyong Wu*[a]

Aqueous multivalent metal batteries represent an attractive option for energy storage. Currently, various metals have been attempted for aqueous battery operation, ranging from divalent metals (zinc, iron, nickel, manganese) to trivalent ones (antimony, indium). However, the fundamental cobalt plating chemistry remains largely neglected and poorly understood, despite its appealing merits in capacity, redox potential, and morphology. Herein, we bridge this knowledge gap by revealing highly reversible Co^{2+}/Co plating reaction in a near-neutral 1 M $CoCl_2$ aqueous electrolyte. Remarkably, cobalt demonstrates exceptional performance, characterized by modest polarization (48 mV), ultrahigh plating efficiency (~99.9%), long lifespan (4,000 hours, 5.5 months), and strong resistance to harsh conditions, including ultrahigh capacities (up to 30 mAh cm^{-2}), ultralow currents (down to 0.05 mA cm^{-2}), and extended storage periods (24-168 hours). The superb performance primarily stems from its closely packed, spherical, and dendrite-free morphology with a minimal surface area. Moreover, cobalt is fully compatible with various cathode materials, enabling high-energy (240 Wh kg^{-1}), high-rate (80 A g^{-1}), and long-cycling (20,000 cycles) batteries. These properties were achieved without delicate optimization of experimental parameters, highlighting the inherent merits of cobalt over other metal candidates. This work unlocks the potential of cobalt for constructing advanced aqueous multivalent batteries.

Introduction

Aqueous multivalent metal batteries (AMMBs) have gained increasing interest for energy storage, due to their utilization of high-capacity metal electrodes in nonflammable and low-cost aqueous electrolytes.[1-3] Among various metal candidates, zinc (Zn) is the most prevalent one; however, the parasitic hydrogen evolution reaction (HER), dendrite growth, and electrode passivation have concurrently constrained the development of Zn metal batteries.[4-8] To circumvent these challenges, researchers have started exploring alternative multivalent metals, spanning from divalent metals like iron (Fe),[9-12] nickel (Ni),[13-15] manganese (Mn),[16-19] copper (Cu),[20-24] tin (Sn),[25-31] and cadmium (Cd),[32] to trivalent metals such as antimony (Sb)[33-38] and indium (In).[39-41] **Figure 1a** highlights some seminal studies in this direction.

The selection of multivalent metal elements is of paramount importance for the overall AMMB performance (**Figure 1b**), which not only impacts the metal anode plating reversibility but also affects the electrolyte stability, thereby influencing the cathode reaction mechanism. In the context of multivalent metals, the Mn^{2+}/Mn redox couple (-1.18 V *vs.* standard hydrogen electrode, SHE) falls outside the water stability window (**Figure 1c**), leading to severe HER, low plating efficiency (73%), and short cycling life (250 hours).[16, 17] The Cu^{2+}/Cu couple, on the other hand, exhibits a substantially high potential (+0.34 V *vs.* SHE) that excludes it as an attractive anode.[20-24] Although Fe, Sn, Ni, Cd, and In exhibit suitable redox potentials (**Figure 1c**) for anode use, these metals also present some noteworthy intrinsic limitations. Both Fe^{2+} and Sn^{2+} ions are excellent reducing agents that can be easily oxidized by dissolved oxygen or high-voltage cathodes. As a result, Fe and Sn metal batteries in a conventional cell design will suffer from electrolyte instability and low voltages (<0.8 V).[9-12, 25-31] Ni metal exhibits large polarization (~400 mV) and thus causes low energy efficiency in full cells.[13-15] Recently, Cd and In metals have demonstrated high efficiency (99.3-99.9%), low polarization (1-5 mV), and long life (1,600-5,000 hours) for plating reactions.[32, 39-41] However, Cd is a very toxic element, whereas In is a highly expensive element (167 USD/kg, **Figure 1d**).

In stark contrast, cobalt (Co) metal batteries have received little attention, although Co is one of the most important elements in lithium-ion batteries (LIBs).[42-46] In fact, Co offers several notable metrics as a compelling anode. Firstly, the Co^{2+}/Co couple (-0.28 V *vs.* SHE) well resides in the water stability window (**Figure 1c**),[47] which effectively mitigates HER and benefits the plating efficiency. Secondly, Co exhibits a high gravimetric capacity of ~910 mAh g^{-1} (**Figure 1e**), surpassing Cu, Zn, Cd, Sn, In, and Sb candidates. This will contribute to high-energy full cells. Thirdly, the acid dissociation constant (K_a) for Co^{2+} is merely $10^{-9.7}$ (**Table S1**), lower than Zn^{2+} (10^{-9}), Fe^{2+} ($10^{-9.4}$), Cu^{2+} ($10^{-7.5}$), Sn ($10^{-3.4}$), and In ($10^{-3.9}$).[48] Consequently, aqueous Co^{2+} electrolytes have low acidity and minimize metal anode corrosion, which can enhance the electrode-electrolyte compatibility and improve the plating efficiency. Despite these underlying merits, Co^{2+}/Co plating chemistry remains largely overlooked and poorly understood in the context of multivalent metals, possibly due to the elemental price concern (**Figure 1d**).[49] However, from a scientific research perspective, it is of crucial importance to investigate the underexplored Co^{2+}/Co plating chemistry, which will not only deepen our fundamental understanding of the multivalent metal electrochemistry but also inspire new innovations for AMMBs.

[a] *Department of Chemistry, University of Puerto Rico-Rio Piedras Campus, San Juan, PR 00925-2537, USA*
[b] *Department of Physics, University of Puerto Rico-Rio Piedras Campus, San Juan, PR, 00925-2537, USA*
**Corresponding author: Dr. Xianyong Wu, xianyong.wu@upr.edu*
Electronic Supplementary Information (ESI) available: [details of any supplementary information available should be included here]. See DOI: 10.1039/x0xx00000x

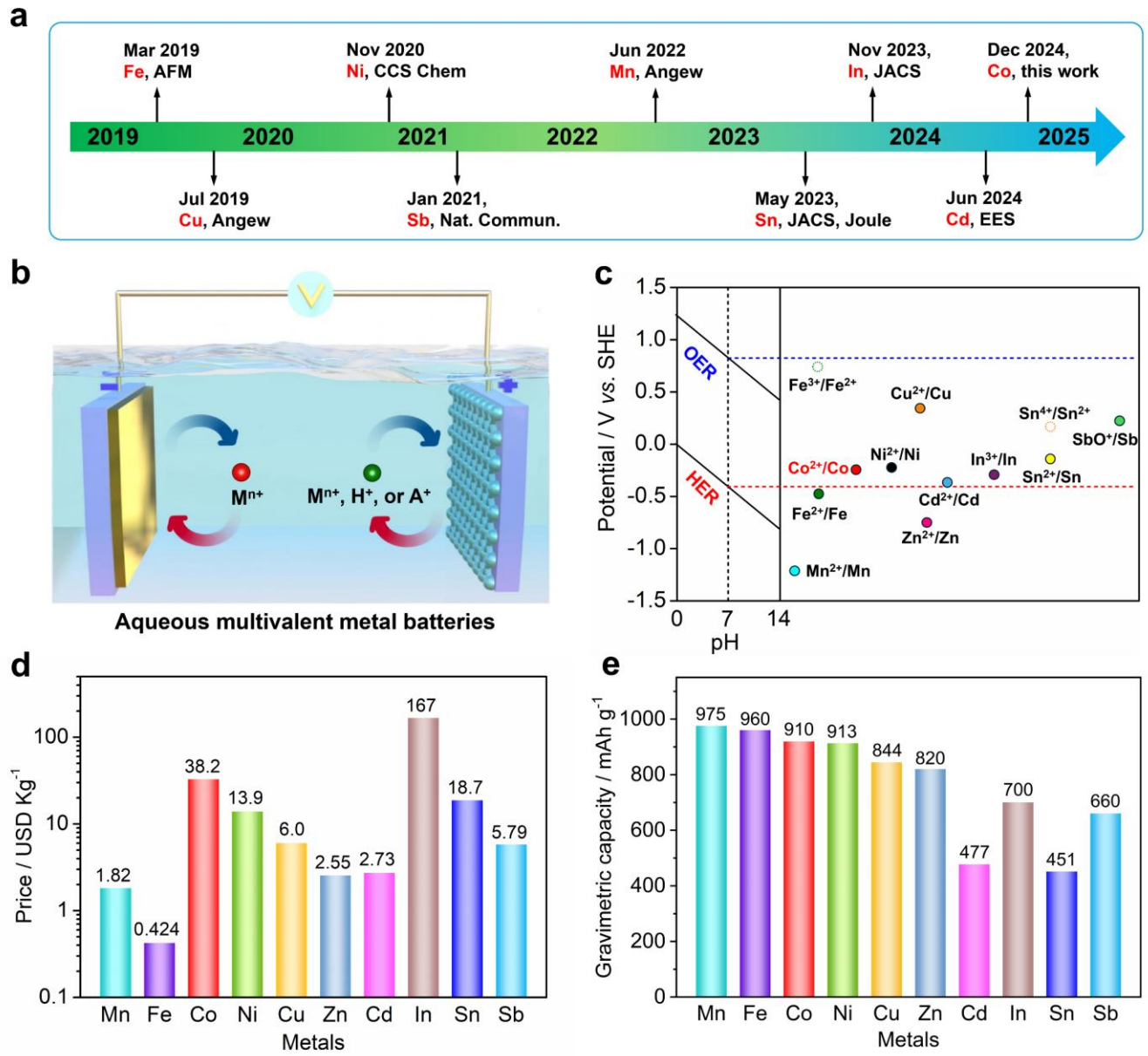

Figure 1. (a) A summary of representative research breakthroughs in AMMBs; (b) The working mechanism of AMMBs, wherein the anode undergoes M^{n+}/M plating reaction, and the cathode hosts multivalent cations (M^{n+}), water-derived protons (H^+), and/or additional cations (A^+) in the electrolyte; (c) The Pourbaix diagram of water and the standard M^{n+}/M electrode potentials (M = Mn, Fe, Co, Ni, Cu, Zn, Cd, In, Sn, and Sb); (d) The elemental price of multivalent metals; (e) The gravimetric capacity of multivalent metals.

In this work, we investigated the Co^{2+}/Co plating chemistry in a near-neutral aqueous electrolyte and revealed its superior electrochemical performance. Specifically, Co exhibits a moderate polarization of ~48 mV, an ultrahigh plating efficiency of ~99.9%, and a long life of 4,000 hours. Even under more challenging conditions, including high capacities, low currents, and extended storage periods, Co still maintains high efficiencies. The impressive performance is likely due to the densely packed and uniformly spherical plating morphology, which minimizes the electrode surface area and inhibits side reactions. We also explored the integration of Co anode with various cathodes and ionic charge carriers, where high-energy, high-rate, and long-cycling full cells were demonstrated.

Results and Discussion

In this work, we tentatively utilized 1 M $CoCl_2$ solution as the electrolyte (purity ≥ 98%, **Figure S1**), although other salts or purity could be further explored (**Figure S2-3**). This electrolyte has a mild pH value of ~5.8, higher than that of 1 M $ZnCl_2$ (pH~4.3), 1 M $CuSO_4$ (pH~4.5), 1 M $InCl_3$ (pH~2.3), and 1 M $SnCl_2$ (pH~1.1), suggesting low electrolyte acidity. Due to the limited availability and ultrahigh price of Co foils (**Table S2**), we opted to use commercial Co powders (**Figure S4-5**) and fabricated thick self-standing films for battery testing (**Figure S6**). **Figure S7** shows the

photo of a home-made Co film, whose mass loading and area capacity is ~60 mg cm^{-2} and ~54 mAh cm^{-2}, respectively.

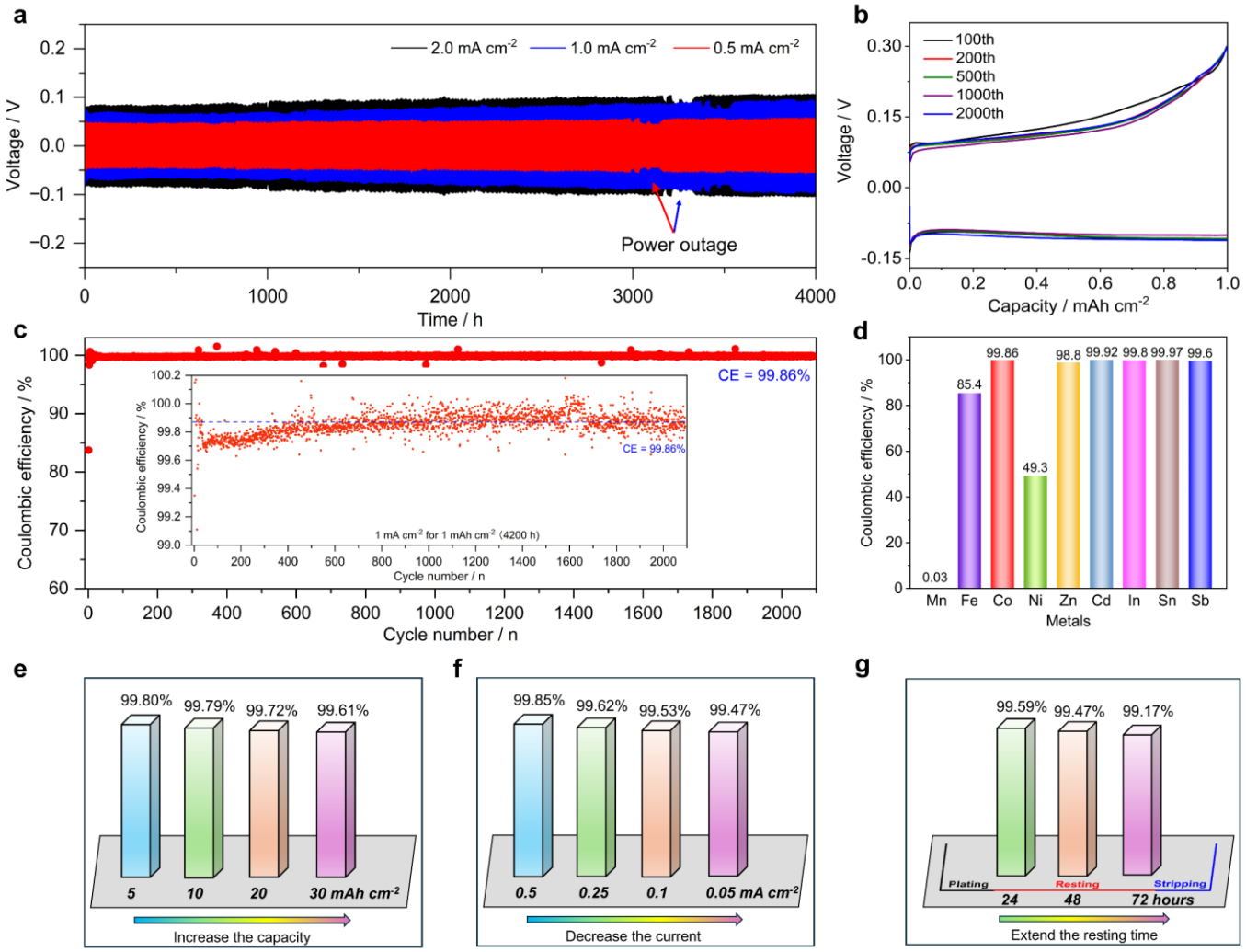

Figure 2. Electrochemical characterization of the Co plating performance. (a) The symmetrical Co‖Co battery performance at different currents (capacity: 0.5 mAh cm^{-2}); (b) GCD curves of the asymmetrical Co‖Cu battery at 1.0 mA cm^{-2} and 1.0 mAh cm^{-2}; (c) The Coulombic efficiency during the cycling, where the inset is an enlarged version; (d) The CE comparison between different multivalent metals under same/comparable conditions; (e) The Co plating efficiency at increased area capacities (current: 1 mA cm^{-2}); (f) The Co plating efficiency at reduced current densities (capacity: 1 mAh cm^{-2}); (g) The Co plating efficiency under different resting periods (1 mA cm^{-2} for 1 mAh cm^{-2}).

We examined the symmetrical Co‖Co battery under various current conditions. After a long period of 4,000 hours (5.5 months), the Galvanostatic charge/discharge (GCD) curves remained stable and flat (**Figure 2a**), indicating a highly reversible Co plating process. Selected GCD curves during cycling are provided in **Figure S8-10**. The polarization is 48 mV at 0.5 mA cm^{-2}, which is comparable to Zn (50 mV) but much lower than Fe (200 mV), Ni (400 mV), and Mn (1100 mV) under similar conditions (**Figure S11**).[9-19] We found that the charge-transfer resistance was as low as ~0.28 ohm (**Figure S12**) in symmetrical cells, which could explain the modest Co polarization. Rate capability tests revealed that the Co polarization moderately increased to 50, 58, 78, 110, and 200 mV at 1, 2, 4, 8, and 10 mA cm^{-2}, respectively (**Figure S13**), suggesting its promise for high-power battery applications. The Co potential is determined as -0.30 V *vs.* SHE (**Figure S14**), close to its standard Co^{2+}/Co potential (-0.28 V). The practical capacity is 850 mAh g^{-1} (**Figure S14**), approaching its theoretical capacity (910 mAh g^{-1}). These results indicate the highly reversible Co^{2+}/Co redox mechanism in the aqueous condition without causing significant electrolyte decomposition or electrode passivation, which is further corroborated by the electrochemical impedance spectroscopy (EIS) and Raman results on the cycled Co electrodes (**Figure S15**). This observation also highlights the difference between aqueous batteries and conventional LIBs, the latter of which is subject to the solid-electrolyte interphase (SEI) formation due to the electrolyte decomposition (**Figure S16**).

Coulombic efficiency (CE) is a critical metric for metal electrodes, which measures the plating reversibility and provides insights into side reactions.[50, 51] To assess this, we utilized a copper (Cu) foil as the substrate and assembled asymmetrical Co‖Cu batteries. **Figures 2b-c** present the battery performance at 1 mA cm^{-2} and 1 mAh cm^{-2}. Impressively, the average CE is as high

as 99.86% (~99.9%) over 2,100 cycles (calendar life: 4,200 hours, 5.8 months), and most CE values fluctuate within a narrow range of ±0.2%, suggesting an exceptionally reversible Co plating behavior. Of note, **Figure 2c** inset is intentionally plotted in a minimal range (99-100.2%) to better show CE datapoints. **Figure 2b** provides GCD curves at the 100th, 200th, 500th, 1000th, and 1900th cycles, which are well overlapped without notable overpotential increment, further confirming the exceptional plating stability.

Such high efficiency was achieved with a pristine 1.0 M electrolyte and a Cu foil, without intricate optimization of electrolytes, additives, or substrates. This represents a significant advantage over other transition metals. For comparison, we tested asymmetrical M||Cu batteries (M = Mn, Fe, Ni, and Zn) under the same condition: 1 mA cm^{-2} for 1 mAh cm^{-2} capacity in the 1 M electrolyte. As shown in **Figure 2d** and **Figure S17**, Mn, Fe, Ni, and Zn delivered lower efficiencies of 0.03%, 85.4%, 49.3%, and 98.8%, respectively, likely due to their inappropriate redox potential (**Figure 1c**) and inferior morphology (**Figure S18**). Meanwhile, the Co efficiency (99.86%) rivals newly developed metals such as In (99.8%),[40] Cd (99.92%),[32] Sn (99.97%),[26] and Sb (99.6%).[33] However, it is worth noting that Co offers a much higher capacity (~910 mAh g^{-1}) than In, Cd, Sn, and Sb metals (451-700 mAh g^{-1}, **Figure 1e**).

More impressively, the Co plating chemistry is robust against harsh conditions, including high capacities, low currents, and extended resting periods, which further underscores the exceptional reversibility of Co metal.

It is generally difficult for metal electrodes to achieve high efficiency at high capacities, due to the increased side reactions and non-uniform plating morphology. Hence, many studies limited the plating capacity to moderate values (0.5-2 mAh cm^{-2}),[52-54] which are insufficient for practical applications. In this case, we gradually increased the Co plating capacity to 5, 10, 20, and eventually 30 mAh cm^{-2} (**Figure S19-20**). The average Co plating efficiency is summarized in **Figure 2e**, which is 99.80%, 99.79%, and 99.72% at 5, 10, and 20 mAh cm^{-2}, respectively. Even at an ultrahigh capacity of 30 mAh g^{-1}, it still retains an impressive CE of 99.61%.

Current density plays a critical role in affecting the plating efficiency, because parasitic side reactions can be kinetically suppressed or masked by high currents.[55-58] Consequently, high currents (1-10 mA cm^{-2}) are widely used to tactically acquire high efficiencies. Herein, we fixed the capacity at 1 mAh cm^{-2} but intentionally decreased the current to 0.5-0.05 mA cm^{-2}. As shown in **Figure 2f**, at moderate currents of 0.25-0.5 mA cm^{-2}, the average CE is 99.62-99.85% and the battery calendar life is more than 4,200 hours (**Figure S21**). When the current decreases to 0.1 mA cm^{-2}, the CE is 99.53% with a long life of 3,000 hours (**Figure S22**). Even at an ultralow current of 0.05 mA cm^{-2}, the average CE still maintains high at 99.47% (**Figure S22**). To our knowledge, such a low current has been rarely used in the AMMB context, which unambiguously reveals the extraordinary Co plating reversibility. **Table S3** summarizes the current, capacity, and efficiency for various multivalent metal batteries, where 0.05 mA cm^{-2} would be the one of the lowest currents used so far.

Aqueous batteries generally suffer from a self-discharge issue. To further push the limit of Co electrode, we introduced a more stringent "plating-resting-stripping" protocol to mimic the practical applications. After the metal plating, we do not immediately strip the battery; instead, we deliberately rest the cell for different periods in ambient conditions (25 °C, ~60% humility, **Figure S23**), so as to amplify potential side reactions during the storage. Impressively, after 24- and 48-hours' resting, the CE remains high at 99.59% and 99.47%, respectively (**Figure 2g** and **Figure S24**). After 72 hours (3 days), the CE can still reach 99.17% (**Figure S25**). We further extended the storage time to 5 and 7 days, and we could still obtain a promising CE of 97.5 and 96.6%, respectively (**Figure S26**). Although the performance may not fully meet the requirements of practical batteries, it is much superior to the widely studied aqueous Zn batteries (**Table S4**). Additionally, with the optimization of electrolytes and other parameters, better performance could be achieved to mitigate the self-discharge challenge. Overall, these aggressive tests collectively validate the exceptional reversibility of Co plating chemistry, which is a salient advantage over other multivalent metals.

The high efficiencies (99.17-99.86%) across various conditions are remarkable, which should originate from the intrinsic properties of Co. Firstly, the Co^{2+}/Co couple (-0.28 V, **Figure 1b**) is within the water stability window, which thermodynamically prevents the HER occurrence. Secondly, the low acidity in the $CoCl_2$ electrolyte (pH~5.8) further mitigates the electrode corrosion, as suggested by the small corrosion current (~0.87 mA cm^{-2}, **Figure 3a**). Lastly but more importantly, the unique spherical Co morphology plays an instrumental role in achieving high efficiency.

Scanning electron microscopy (SEM) was utilized to investigate Co morphology evolution at representative stages (**Figure 3b**). At 0.2 mAh cm^{-2}, the initial Co deposits appear as individually dispersed particles, with an average size of 1.5-2 µm. With the proceeding of plating (0.5 and 1 mAh cm^{-2}), these Co particles form a regular, uniform, and spherical "meatball-like" morphology (**Figure 3c-e**), where smaller metal particles are closely packed together. The aggregate size increases to 5 and 10 µm at 0.5 and 1 mAh cm^{-2} capacity, respectively (**Figure S27**). Energy dispersive spectroscopy (EDS) detects Co and Cu elements only (**Figure 3i**), suggesting the deposit purity. Besides, the X-ray diffraction (XRD) pattern of the deposit is well attributed to Co metal (PDF#04-004-6150, **Figure S28**), and there are no additional peaks, suggesting the absence of electrolyte decomposition or salt precipitation side reactions. Raman spectroscopy (**Figure S29**) suggests that the Co deposit surface does not contain electrolyte decomposition compounds. Of note, it is common to observe zinc salt precipitation during plating, due to the parasitic HER reaction and local pH change.[59-61]

We highlight that the spherical, micro-sized, and closely packed morphology has been rarely reported among multivalent metals,[16-36] which directly contribute to the superior Co plating efficiency. It is well accepted that micro-sized sphere morphology is particularly advantageous for battery electrodes,[62-64] because it effectively minimizes the electrode surface area compared to other geometric morphologies. Hence, plated Co metals exhibit a

minimal contact area with electrolytes, thus mitigating parasitic side reactions. Additionally, the spherical morphology boosts the particle stacking efficiency, which in turn increases the electrode tap density. For instance, $LiMn_2O_4$, a commercial LIB cathode, adopts a similar micro-sphere morphology to reduce its surface area and increase its tap density (**Figure S30**).

The Co stripping process is highly reversible. At 0.5 mAh cm^{-2}, the aggregated particles start losing internal connections, and some gaps emerge between metal clusters (**Figure 3f**). The particle size reduces to ~5 μm (**Figure S31**). At 0.8 mAh cm^{-2}, Co dissolution becomes more pronounced (**Figure 3g** and **Figure S31**), and the residual particles appear irregular and highly porous. At the end of charging, all Co metals completely dissolve, leaving behind a clean Cu foil surface (**Figure 3h** and **Figure S32**), suggesting a highly reversible stripping process.

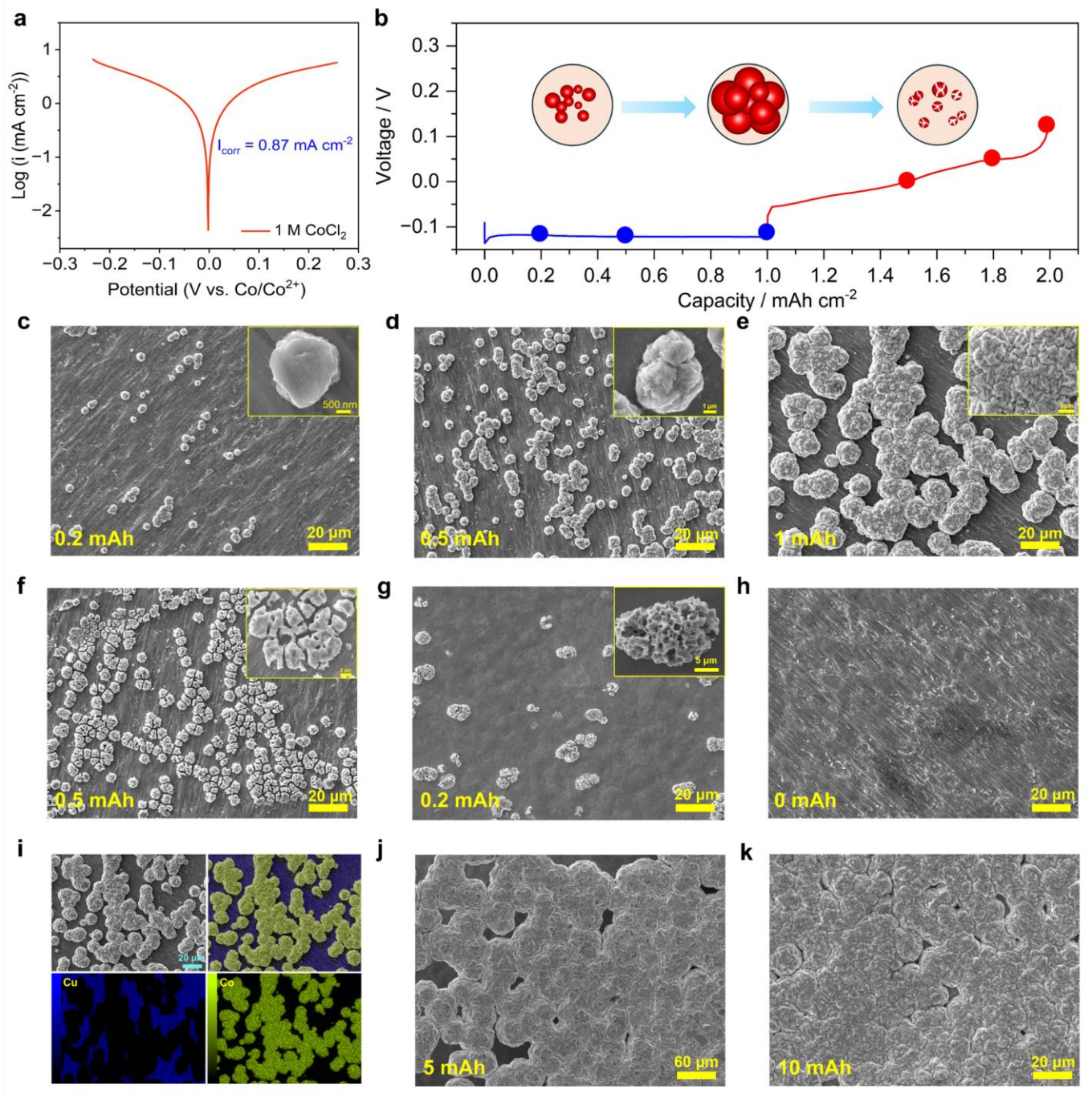

Figure 3. The Tafel plot and morphology evolution of the Co metal. (a) The Tafel curve of Co in 1 M $CoCl_2$; (b) A typical GCD curve with schemes to illustrate the morphology change; (c-e) SEM images at plating capacities of 0.2, 0.5, and 1 mAh cm^{-2}; (f-h) SEM images at stripping capacities of 0.5, 0.8, and ~1 mAh cm^{-2}; (i) The EDS mapping of plated Co at 1 mAh cm^{-2}. (j-k) SEM images at plating capacities of 5 and 10 mAh cm^{-2}. The current is 1 mA cm^{-2}.

We examined the morphology of Co at higher capacities. Notably, Co demonstrated a similar spherical, densely packed, and dendrite-free morphology (**Figure 3j-k**), which explains the observed high efficiencies. We also tested the XRD pattern of the cycled Co electrode, which maintained a nearly identical pattern to the original one (**Figure S33**). These results clearly indicate the superb Co plating chemistry in a simple 1 M aqueous electrolyte.

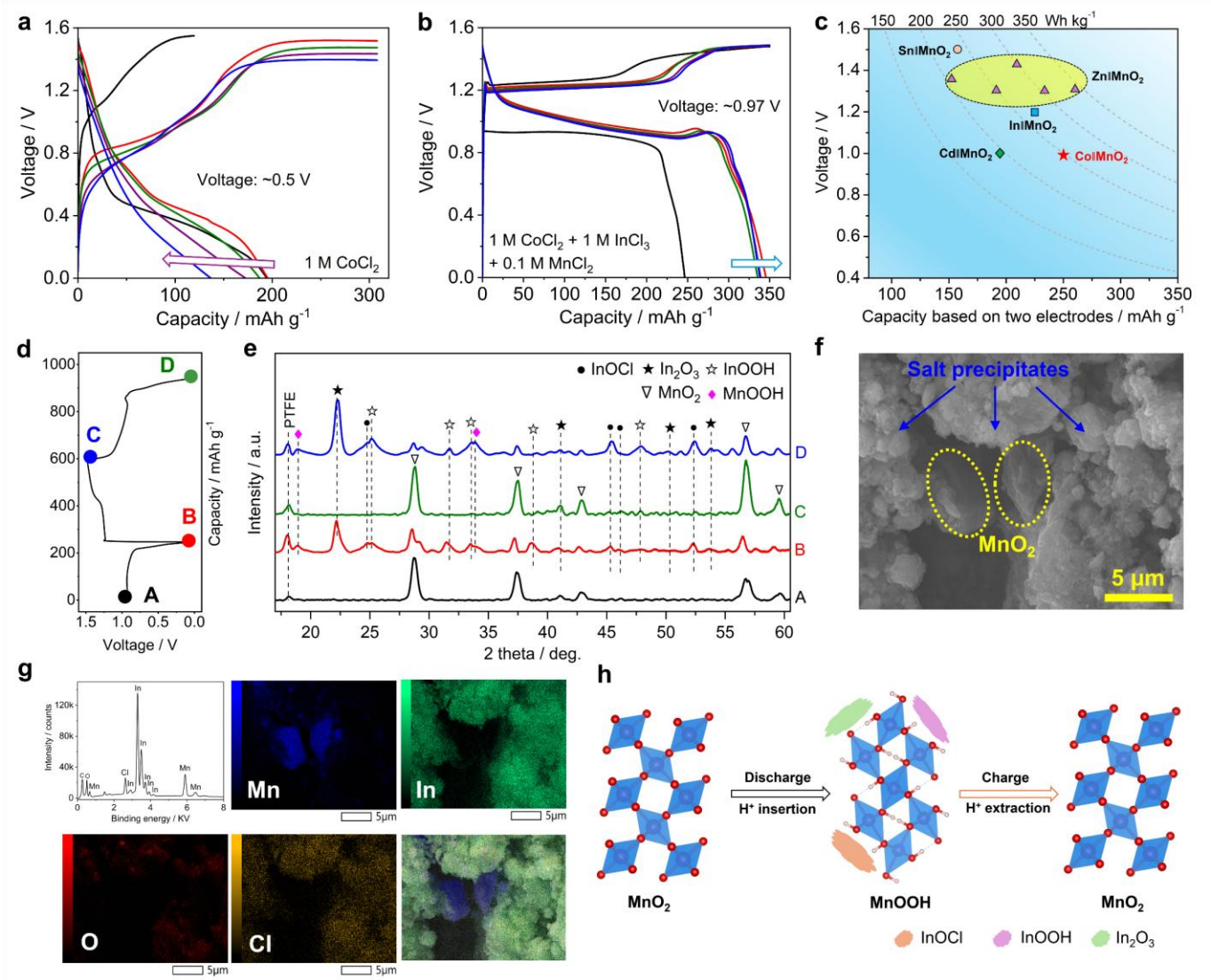

Figure 4. The Co‖MnO_2 battery performance and working mechanism. (a) GCD curves in the 1 M $CoCl_2$ electrolyte; (b) GCD curves in the 1 M $CoCl_2$ + 1 M $InCl_3$ + 0.1 M $MnCl_2$ electrolyte; (c) The energy density comparison between Co‖MnO_2 and other metal‖MnO_2 batteries; (d-e) *Ex-situ* XRD patterns of the MnO_2 electrode; (f) SEM image of the discharged MnO_2 (point B); (g) EDS mapping analysis of the discharged electrode (point B); (h) The scheme of the cathode reaction mechanism.

Motivated by the excellent Co anode performance, we aimed to develop high-capacity, high-rate, and long-cycling cathodes for Co metal batteries. We selected a manganese dioxide cathode (MnO_2, **Figure S34**), due to its low cost and high capacity. **Figure 4a** shows the Co‖MnO_2 battery performance in 1 M $CoCl_2$, where a good capacity (~195 mAh g^{-1}) and a modest voltage (~0.5 V) is delivered. However, this battery undergoes fast capacity fading, likely due to the manganese dissolution in mild pH conditions (**Figure S35**). To address this issue, we proposed decreasing the electrolyte pH and adding extra Mn^{2+} salts. Herein, 1 M $InCl_3$ and 0.1 $MnCl_2$ were introduced to the pristine 1 M $CoCl_2$ electrolyte. Note that In^{3+} ions can maintain a mildly acidic environment due to the In^{3+}/H_2O chemical equilibrium.[41] Meanwhile, In^{3+} will not be reduced by cobalt, since the In^{3+}/In potential (-0.34 V) is lower than Co^{2+}/Co (-0.28 V). The final pH for the hybrid electrolyte is ~3.1, lower than the pristine $CoCl_2$ (~5.8), which will facilitate proton (H^+) insertion in β-MnO_2.

As expected, the Co‖MnO_2 battery exhibits an improved cell performance, including a higher capacity (~340 mAh g^{-1}), a higher voltage (~0.97 V), and more overlapped GCD curves (**Figure 4b**). Based on the voltage and the electrode capacities (MnO_2: 340 mAh g^{-1}; Co: 910 mAh g^{-1}), this Co‖MnO_2 battery could potentially achieve high energy density of ~240 Wh kg^{-1}. This energy is comparable to other AMMBs using the MnO_2 cathode (**Figure 4c** and **Table S5**), including the prevalent Zn‖MnO_2 batteries[65-69] and newly studied Sn‖MnO_2 (244 Wh kg^{-1}),[28] Cd‖MnO_2 (188 Wh kg^{-1}),[32] and In‖MnO_2 batteries (273 Wh kg^{-1}).[39] Besides the high

energy, this battery exhibits a reasonable rate capability and cycling life (**Figure S36**).

To understand the battery working mechanism, we conducted *ex-situ* XRD and SEM analysis on MnO_2 at different charge/discharge states (**Figure 4d**). After the initial discharge (state B), there is a significant change in the XRD pattern, where new peaks attributed to MnOOH, InOOH, In_2O_3, and InOCl are detected (**Figure 4e**). This result agrees with the previous In‖MnO_2 research,[25] wherein H^+ insertion in MnO_2 causes the local pH change, leading to the In^{3+} salt co-precipitation. SEM and EDS tests reveal that MnO_2 is surrounded by In/Cl/O elements (**Figure 4f-g**), which further support the H^+ insertion and salt precipitation. The salt precipitation should be a mixture of InOOH, In_2O_3, and InOCl (**Figure 4f**), as suggested by the XRD analysis.

During charging (state C), the XRD pattern well matches that of the initial β-MnO_2 (**Figure 4e**). Meanwhile, most precipitation peaks disappear, suggesting a reversible dissolution process. Upon discharge (state D), the XRD pattern is akin to that in the first cycle (state B), suggesting the re-formation of MnOOH and the resultant salt precipitation. Overall, the Co‖MnO_2 battery operates on a proton insertion reaction (**Figure 4h**), which changes the local electrolyte pH and precipitates In^{3+} ions accordingly. The H^+ insertion mechanism accounts for the improved capacity and voltage, because the hybrid electrolyte contains a much higher H^+ concentration than pristine $CoCl_2$. Consequently, the H^+ insertion reaction is more favorable to take place, leading to enhanced electrochemical performance.

We also add that the detailed working mechanism of MnO_2 in aqueous multivalent metal batteries remains a controversial and debated topic, where various explanations have been proposed, including H^+ insertion,[66] multivalent ion insertion,[70,71] H^+ and multivalent ion co-insertion,[65] and manganese dissolution-redeposition.[72,73] Among them, H^+ insertion is usually believed to be a prevalent reaction, due to the thermodynamic preference and fast reaction kinetics.[66] Our results suggest that the H^+ insertion plays a major role, but other mechanisms may also contribute to the high capacity and stable cycling, especially considering that Mn^{2+} ions are pre-added to the electrolyte. During charging, some Mn^{2+} ions may be oxidized at the cathode and deposited on the MnO_2 surface (**Figure S37**);[72,73] however, Mn^{2+} ions will not be reduced by the Co metal anode (**Figure S37**), due to their redox potential differences (Co^{2+}/Co: -0.28 V; Mn^{2+}/Mn: -1.18 V).[47] In future studies, more advanced techniques will be exploited to gain deeper insight into the MnO_2 working mechanism, such as high-resolution transmission electron microscopy and *in-situ* XRD experiments.

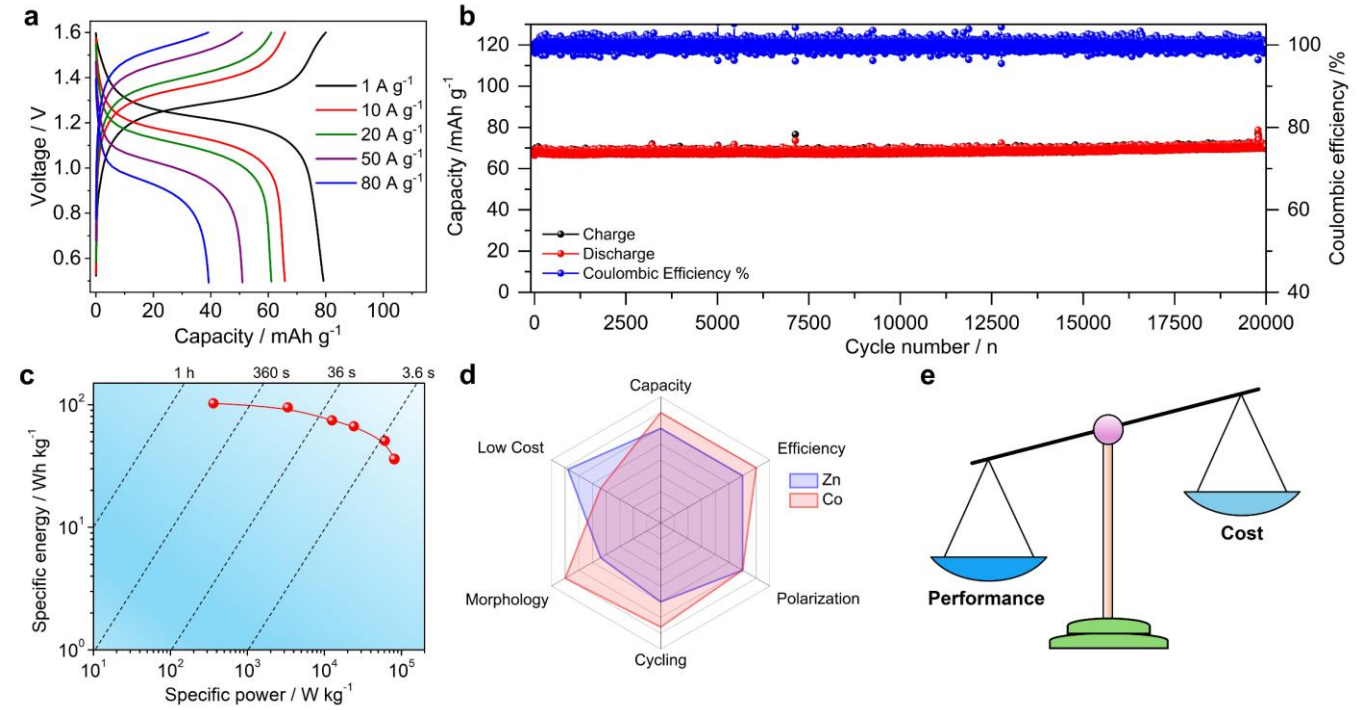

Figure 5. Characterization and analysis of Co-based batteries. (a) Rate performance of the Co‖$KCuFe(CN)_6$ hybrid battery; (b) Cycling performance of the hybrid battery at 10 A g^{-1}; (c) Ragone plot of the hybrid battery; (d) Radar plot comparison between Co and Zn; (e) A scheme to delineate the performance over cost.

In addition to the high-energy Co‖MnO_2 battery, we sought to demonstrate high-power and long-cycling Co based hybrid batteries. In the hybrid cell design (**Figure 1b**), the Co anode works on the reversible Co^{2+}/Co plating reaction, whereas the cathode selectively hosts additive cations in the electrolyte. This principle facilitates the use of various cathodes and ionic charge carriers, which enables Co metal batteries with tunable performance (**Figure S38-39**). Here we selected an open framework Prussian blue of $KCuFe(CN)_6$ (**Figure S40**), owing to its high structural preference toward K^+ over other cations.

In the 1 M $CoCl_2$ + 1 M KCl electrolyte, the Co‖$KCuFe(CN)_6$ battery exhibits a stable output voltage of 1.25 V and a reasonable capacity of ~80 mAh g^{-1} (**Figure S41**), corresponding to a specific energy of ~100 Wh kg^{-1} based on the cathode mass. The capacity is close to its theoretical capacity (~85 mAh g^{-1})

based on the Fe^{3+}/Fe^{2+} redox couple. Impressively, this battery demonstrates an extraordinary rate capability (**Figure 5a**), where the discharge capacity is 79, 65, 61, and 52 mAh g^{-1} at 1, 10, 20, and 50 A g^{-1}, respectively. Even at an ultrahigh current of 80 A g^{-1}, approximately 1000 C rate, the discharge capacity still reaches 39 mAh g^{-1}, corresponding to 46% capacity utilization. Besides, this battery manifests an exceptional cycling life, with nearly 100% capacity retention over 20,000 cycles (**Figure 5b**). We also provide the Ragone plot to show the energy-power correlation (**Figure 5c**), where a specific energy of 36 Wh kg^{-1} is attainable at ultrahigh power of 80,955 W kg^{-1} (less than 3.6 seconds). Such a high power should result from the high conductivity in the 1 M $CoCl_2$ + 1 M KCl electrolyte (**Figure S42**) and pseudocapacitive K-insertion behavior in the $KCuFe(CN)_6$ cathode (**Figure S43**).

It is worth noting that this material operates *via* K^+ ion insertion in its bulk structure other than the surface absorption, as indicated by the reversible lattice expansion/contraction in *ex-situ* XRD analysis (**Figure S44**). Besides, $KCuFe(CN)_6$ is a well-known battery material in the aqueous battery context,[74,75] which demonstrates typical S-shaped GCD curves related to the K-ion insertion. Therefore, it is appropriate to label this system as a high-rate battery, despite its pseudocapacitance behavior. The K-insertion reaction is expressed as:

$KCuFe^{III}(CN)_6 + K^+ + e^- = K_2CuFe^{II}(CN)_6$

Overall, cobalt metal holds a significant promise for constructing high-energy, high-power, and long-cycling aqueous batteries for energy storage. Compared with the widely used Zn metal (**Figure 5d**), Co demonstrates remarkable advantages in plating morphology, achieving close-packed, micro-spherical, and dendrite-free morphology under simple conditions without elaborate optimization of electrolytes, additives, or substrates. The unique morphology plays a critical role in delivering ultrahigh efficiency and exceptional life, even under various challenging conditions. Consequently, aqueous Co metal batteries could be a promising alternative for energy storage, due to their superior morphology, efficiency, and cycling merits.

Lastly, we emphasize that battery research is never monolithic; it encompasses a wide range of interconnected parameters, including energy, power, cycling, safety, cost, and environmental impact, *etc.* While cobalt is expensive, its comprehensive and exceptional battery performance (efficiency, morphology, and cycling life) has the potential to outweigh concerns about cost (**Figure 5e**). Furthermore, this work serves as a fundamental study of Co plating chemistry, which offers valuable insights into the redox behavior of multivalent metals. By investigating the fundamental aspects of cobalt plating reaction and its feasibility for metal batteries, this work contributes to a broader understanding that could unlock unexpected pathways for future innovations in energy storage.

Conclusions

We investigated the fundamental properties of the underexplored Co plating chemistry and demonstrated its potential as high-efficiency and long-life metal anode for aqueous multivalent batteries. With a conventional 1 M $CoCl_2$ electrolyte and a regular Cu foil substrate, the Co electrode exhibited exceptionally high efficiencies (99.17-99.86%) across various conditions (0.05-1 mA cm^{-2}; 1-30 mAh cm^{-2}; 24-72 hours' resting), far surpassing other multivalent metal electrodes. This remarkable performance is rooted in the intrinsic properties of Co, including a suitable redox potential, a near-neutral electrolyte, and a micro-sized, closely packed, and spherical plating morphology. Additionally, we explored full-cell applications with different cathodes and ionic charge carriers, where high-energy, high-rate, and long-cycling aqueous Co metal batteries were successfully demonstrated. These findings not only advance the performance of aqueous multivalent metal batteries but also deepen our understanding of the intriguing cobalt metal redox chemistry.

Author Contributions

All authors have given permission for the final version of this manuscript. Conceptualization: X. Wu; data curation and formal analysis: S. Chang, W. Hou, A. Valle-Perez, I. Ullah, X. Du; visualization: X. Wu; resources: L. Cunci, G. Morell and X. Wu; writing-original draft, review, and editing: S. Chang, X. Wu.

Conflicts of interest

There are no conflicts to declare.

Acknowledgements

The authors thank the financial support from the NSF Center for the Advancement of Wearable Technologies (grant no. 1849243), NASA MIRO PR-SPRInT (grant no. 80NSSC19M0236), and NASA EPSCoR (grant no. 80NSSC23M0189). The authors also thank Jiayi Xue in Konkuk University for preparing Figure 1b and TOC figure in this paper.

Notes and references

1 D. Chao, W. Zhou, F. Xie, C. Ye, H. Li, M. Jaroniec and S.-Z. Qiao, *Sci. Adv.*, 2020, **6**, eaba4098.
2 X. Tang, D. Zhou, B. Zhang, S. Wang, P. Li, H. Liu, X. Guo, P. Jaumaux, X. Gao and Y. Fu, *Nat. Commun.*, 2021, **12**, 2857.
3 Y. Sui and X. Ji, *Angew. Chem. Int. Ed.*, 2024, **63**, e202312585.
4 H. Wang, R. Tan, Z. Yang, Y. Feng, X. Duan and J. Ma, *Adv. Energy Mater.*, 2021, **11**, 2000962.
5 M. Yan, P. He, Y. Chen, S. Wang, Q. Wei, K. Zhao, X. Xu, Q. An, Y. Shuang and Y. Shao, *Adv. Mater.*, 2018, **30**, 1703725.
6 H. Li, R. Zhao, W. Zhou, L. Wang, W. Li, D. Zhao and D. Chao, *JACS Au*, 2023, **3**, 2107-2116.
7 H. Liu, Z. Xin, B. Cao, Z. Xu, B. Xu, Q. Zhu, J. L. Yang, B. Zhang and H. J. Fan, *Adv. Funct. Mater.*, 2024, **34**, 2309840.
8 Q. Yang, Q. Li, Z. Liu, D. Wang, Y. Guo, X. Li, Y. Tang, H. Li, B. Dong and C. Zhi, *Adv. Mater.*, 2020, **32**, 2001854.
9 X. Wu, A. Markir, Y. Xu, C. Zhang, D. P. Leonard, W. Shin and X. Ji, *Adv. Funct. Mater.*, 2019, **29**, 1900911.
10 Z. He, F. Xiong, S. Tan, X. Yao, C. Zhang and Q. An, *Mater. Today Adv.*, 2021, **11**, 100156.

11 J. Liu, D. Dong, A. L. Caro, N. S. Andreas, Z. Li, Y. Qin, D. Bedrov and T. Gao, *ACS Cent. Sci.*, 2022, **8**, 729-740.
12 C. Bai, H. Jin, Z. Gong, X. Liu and Z. Yuan, *Energy Storage Mater.*, 2020, **28**, 247-254.
13 J. Zhao, X. Yang, S. Li, N. Chen, C. Wang, Y. Zeng and F. Du, *CCS Chem.*, 2021, **3**, 2498-2508.
14 M. Wang, Y. Meng, P. Gao, K. Li, Z. Liu, Z. Zhu, M. Ali, T. Ahmad, N. Chen and Y. Yuan, *Adv. Mater.*, 2023, **35**, 2305368.
15 S. Li, X. Yang, X. Li, Z. Wei, M. Li, F. Hu, Y. Xie, X. Meng, C. Wang and G. Chen, *Chem. Eng. J.*, 2021, 413, 127441.
16 M. Wang, Y. Meng, Y. Xu, N. Chen, M. Chuai, Y. Yuan, J. Sun, Z. Liu, X. Zheng and Z. Zhang, *Energy Environ. Sci.*, 2023, **16**, 5284-5293.
17 Q. Yang, X. Qu, H. Cui, X. He, Y. Shao, Y. Zhang, X. Guo, A. Chen, Z. Chen and R. Zhang, *Angew. Chem. Int. Ed.*, 2022, **61**, e202206471.
18 S. Bi, Y. Zhang, S. Deng, Z. Tie and Z. Niu, *Angew. Chem. Int. Ed.*, 2022, **61**, e202200809.
19 S. Bi, S. Wang, F. Yue, Z. Tie and Z. Niu, *Nat. Commun.*, 2021, **12**, 6991.
20 H. Cai, S. Bi, R. Wang, L. Liu and Z. Niu, *Angew. Chem. Int. Ed.*, 2022, **61**, e202205472.
21 G. Liang, F. Mo, Q. Yang, Z. Huang, X. Li, D. Wang, Z. Liu, H. Li, Q. Zhang and C. Zhi, *Adv. Mater.*, 2019, **31**, 1905873.
22 J. Zhang, X. Zhang, C. Xu, H. Yan, Y. Liu, J. Xu, H. Yu, L. Zhang and J. Shu, *Adv. Energy Mater.*, 2022, **12**, 2103998.
23 C. Dai, L. Hu, H. Chen, X. Jin, Y. Han, Y. Wang, X. Li, X. Zhang, L. Song and M. Xu, *Nat. Commun.*, 2022, **13**, 1863.
24 X. Wu, A. Markir, L. Ma, Y. Xu, H. Jiang, D. P. Leonard, W. Shin, T. Wu, J. Lu and X. Ji, *Angew. Chem. Int. Ed.*, 2019, **58**, 12640-12645.
25 W. Zhou, S. Ding, D. Zhao and D. Chao, *Joule*, 2023, **7**, 1104-1107.
26 S. Chang, W. Hou, A. Del Valle-Perez, I. Ullah, S. Qiu, J. L. Rodriguez, L. M. Díaz-Vázquez, L. Cunci, G. Morell and X. Wu, *Angew. Chem. Int. Ed.*, 2025, **64**, e202414346.
27 Y. Yao, Z. Wang, Z. Li and Y. C. Lu, *Adv. Mater.*, 2021, **33**, 2008095.
28 H. Zhang, D. Xu, F. Yang, J. Xie, Q. Liu, D.-J. Liu, M. Zhang, X. Lu and Y. S. Meng, *Joule*, 2023, **7**, 971-985.
29 Z. Yu, Q. Wang, Y. Li, F. Zhang, X. Ma, X. Zhang, Y. Wang, J. Huang and Y. Xia, *Joule*, 2024, **8**, 1063-1079.
30 D. Xu, H. Zhang, J. Xie, L. Zhou, F. Yang, J. Ma, Y. Yu, G. Wang and X. Lu, *Adv. Mater.*, 2024, **36**, 2408067.
31 W. Zhou, M. Song, P. Liang, X. Li, X. Liu, H. Li, T. Zhang, B. Wang, R. Zhao and Z. Zhao, *J. Am. Chem. Soc.*, 2023, **145**, 10880-10889.
32 S. Katiyar, S. Chang, I. Ullah, W. Hou, A. Conde-Delmoral, S. Qiu, G. Morell and X. Wu, *Energy Environ. Sci.*, 2024, **17**, 4770-4779.
33 H. Zhang, Q. Liu, D. Zheng, F. Yang, X. Liu and X. Lu, *Nat. Commun.*, 2021, **12**, 14.
34 Y. Yu, R. Qin, X. Shi, J. Xie, T. H. Lu and X. Lu, *Batter. Energy*, 2023, **2**, 20230016.
35 F. Wang, J. Xie, D. Zheng, F. Yang, H. Zhang and X. Lu, *Adv. Mater.*, 2022, **34**, 2200085.
36 Q. Liu, H. Zhang, J. Xie, F. Yang, Z. Yang, X. Liu, H. Wu, Q. Liu and X. Lu, *Nano Energy*, 2023, **113**, 108567.
37 Y. Yu, J. Xie, L. Zhou, F. Yang, H. Zhang, X. Liu, P. Yu and X. Lu, *Energy Storage Mater.*, 2022, **49**, 529-536.
38 P. Zhang, J. Xie, F. Yang, X. Shi, Y. Yu and X. Lu, *J. Mater. Sci. Technol.*, 2022, **131**, 60-67.
39 S. Chang, J. F. F. Gomez, S. Katiyar, G. Morell and X. Wu, *J. Am. Chem. Soc.*, 2023, **145**, 24746-24754.
40 S. Chang, L. Lu, I. Ullah, W. Hou, J. F. Florez Gomez, A. Conde‐Delmoral, C. M. Font Marin, G. Morell, Z. Chen and X. Wu, *Adv. Funct. Mater.*, 2024, **34,** 2407342.
41 S. Chang, W. Hou, A. Conde-Delmoral, I. Ullah, J. F. F. Gomez, G. Morell, and X. Wu, *Nanoscale*, 2025, **17**, 855-863.
42 S Lee, and A Manthiram, *ACS Energy Lett.* 2022, **7**, 3058–3063.
43 Y. Lyu, X. Wu, K. Wang, Z. Feng, T. Cheng, Y. Liu, M. Wang, R. Chen, L. Xu and J. Zhou, *Adv. Energy Mater.*, 2021, **11**, 2000982.
44 A. Manthiram, *Nat. Commun.*, 2020, **11**, 1550.
45 G.-T. Park, H.-H. Ryu, T.-C. Noh, G.-C. Kang and Y.-K. Sun, *Mater. Today*, 2022, **52**, 9-18.
46 G. W. Nam, N.-Y. Park, K.-J. Park, J. Yang, J. Liu, C. S. Yoon and Y.-K. Sun, *ACS Energy Lett.*, 2019, **4**, 2995-3001.
47 S. G. Bratsch, *J. Phys. Chem. Ref. Data*, 1989, **18**, 1-21.
48 D. C. Harris, *Quant. Chem. Anal.*, Macmillan, 2010.
49 S. Lee and A. Manthiram, *ACS Energy Lett.*, 2022, **7**, 3058-3063.
50 J. Xiao, Q. Li, Y. Bi, M. Cai, B. Dunn, T. Glossmann, J. Liu, T. Osaka, R. Sugiura and B. Wu, *Nat. Energy*, 2020, **5**, 561-568.
51 B. D. Adams, J. Zheng, X. Ren, W. Xu and J. G. Zhang, *Adv. Energy Mater.*, 2018, **8**, 1702097.
52 Z. Wang, J. Huang, Z. Guo, X. Dong, Y. Liu, Y. Wang and Y. Xia, *Joule*, 2019, **3**, 1289-1300.
53 53. J. Zheng, D. C. Bock, T. Tang, Q. Zhao, J. Yin, K. R. Tallman, G. Wheeler, X. Liu, Y. Deng and S. Jin, *Nat. Energy*, 2021, **6**, 398-406.
54 54. Y. An, Y. Tian, K. Zhang, Y. Liu, C. Liu, S. Xiong, J. Feng and Y. Qian, *Adv. Funct. Mater.*, 2021, **31**, 2101886.
55 C. Zhang, J. Holoubek, X. Wu, A. Daniyar, L. Zhu, C. Chen, D. P. Leonard, I. A. Rodríguez-Pérez, J.-X. Jiang and C. Fang, *Chem. Commun.*, 2018, **54**, 14097-14099.
56 L. Ma, M. A. Schroeder, O. Borodin, T. P. Pollard, M. S. Ding, C. Wang and K. Xu, *Nat. Energy*, 2020, **5**, 743-749.
57 Y. Sui and X. Ji, *Chem. Rev.*, 2021, **121**, 6654-6695.
58 C. Zhang, W. Shin, L. Zhu, C. Chen, J. C. Neuefeind, Y. Xu, S. I. Allec, C. Liu, Z. Wei and A. Daniyar, *Carbon Energy*, 2021, **3**, 339-348.
59 A. Bayaguud, Y. Fu and C. Zhu, *J. Energy Chem.*, 2022, **64**, 246-262.
60 K. Ouyang, S. Chen, W. Ling, M. Cui, Q. Ma, K. Zhang, P. Zhang and Y. Huang, *Angew. Chem.*, 2023, **135**, e202311988.
61 M. Zhang, H. Hua, P. Dai, Z. He, L. Han, P. Tang, J. Yang, P. Lin, Y. Zhang and D. Zhan, *Adv. Mater.*, 2023, **35**, 2208630.
62 F. Wu, G. Tan, J. Lu, R. Chen, L. Li and K. Amine, *Nano Lett.*, 2014, **14**, 1281-1287.
63 X. Deng, R. Zhang, K. Zhou, Z. Gao, W. He, L. Zhang, C. Han, F. Kang and B. Li, *Energy Environ. Mater.*, 2023, **6**, e12331.
64 Z. Xu, Z. Jiang, C. Kuai, R. Xu, C. Qin, Y. Zhang, M. M. Rahman, C. Wei, D. Nordlund and C.-J. Sun, *Nat. Commun.*, 2020, **11**, 83.
65 W. Sun, F. Wang, S. Hou, C. Yang, X. Fan, Z. Ma, T. Gao, F. Han, R. Hu and M. Zhu, *J. Am. Chem. Soc.*, 2017, **139**, 9775-9778.
66 H. Pan, Y. Shao, P. Yan, Y. Cheng, K. S. Han, Z. Nie, C. Wang, J. Yang, X. Li and P. Bhattacharya, *Nat. Energy*, 2016, **1**, 1-7.
67 J. Huang, Z. Wang, M. Hou, X. Dong, Y. Liu, Y. Wang and Y. Xia, *Nat. Commun.*, 2018, **9**, 2906.
68 Y. Fu, Q. Wei, G. Zhang, X. Wang, J. Zhang, Y. Hu, D. Wang, L. Zuin, T. Zhou and Y. Wu, *Adv. Energy Mater.*, 2018, **8**, 1801445.
69 Q. Zhao, W. Huang, Z. Luo, L. Liu, Y. Lu, Y. Li, L. Li, J. Hu, H. Ma and J. Chen, *Sci. Adv.*, 2018, **4**, eaao1761.
70 C. Xu, B. Li, H. Du and F. Kang, *Angew. Chem. Int. Ed.*, 2012, **51**, 933-935.

71 N. Zhang, F. Cheng, J. Liu, L. Wang, X. Long, X. Liu, F. Li and J. Chen, *Nat. Commun.*, 2017, **8**, 1-9.
72 T.-H. Wu, Y.-Q. Lin, Z. D. Althouse and N. Liu, *ACS Appl. Energy Mater.*, 2021, **4**, 12267-12274.
73 V. R. Kankanallu, X. Zheng, D. Leschev, N. Zmich, C. Clark, C.-H. Lin, H. Zhong, S. Ghose, A. M. Kiss and D. Nykypanchuk, *Energy Environ. Sci.*, 2023, **16**, 2464-2482.
74 C. Wessells, A. Huggins, Y. Cui, Nat. Commun., 2011, **2**, 550.
75 P. Jiang, H. Shao, L. Chen, J. Feng, Z. Liu, J. Mater. Chem. A, 2017, **5**, 16740-16747.

The data supporting this article have been included as part of the Supplementary Information.